A Discussion on the Errors in the Surface Heat Fluxes Simulated by a Coupled GCM

JIN-YI YU AND CARLOS R. MECHOSO

Department of Atmospheric Sciences, University of California, Los Angeles, Los Angeles, California

ABSTRACT

This paper contrasts the sea surface temperature (SST) and surface heat flux errors in the Tropical Pacific simulated by the University of California, Los Angeles, coupled atmosphere–ocean general circulation model (CGCM) and by its atmospheric component (AGCM) using prescribed SSTs. The usefulness of such a comparison is discussed in view of the sensitivities of the coupled system.

Off the equator, the CGCM simulates more realistic surface heat fluxes than the AGCM, except in the eastern Pacific south of the equator where the coupled model produces a spurious intertropical convergence zone. The AGCM errors are dominated by excessive latent heat flux, except in the stratus regions along the coasts of California and Peru where errors are dominated by excessive shortwave flux. The CGCM tends to balance the AGCM errors by either correctly decreasing the evaporation at the expense of cold SST biases or erroneously increasing the evaporation at the expense of warm SST biases.

At the equator, errors in simulated SSTs are amplified by the feedbacks of the coupled system. Over the western equatorial Pacific, the CGCM produces a cold SST bias that is a manifestation of a spuriously elongated cold tongue. The AGCM produces realistic values of surface heat flux. Over the cold tongue in the eastern equatorial Pacific, the CGCM simulates realistic annual variations in SST. In the simulation, however, the relationship between variations in SST and surface latent heat flux corresponds to a negative feedback, while in the observation it corresponds to a positive feedback. Such an erroneous feature of the CGCM is linked to deficiencies in the simulation of the cross-equatorial component of the surface wind. The reasons for the success in the simulation of SST in the equatorial cold tongue despite the erroneous surface heat flux are examined.

1. Introduction

The seasonal cycle of the atmosphere–ocean system is determined by complex interactions and feedbacks between elements of the system. The simulation of the seasonal cycle by a coupled GCM (CGCM) is thus highly sensitive to the successes/deficiencies of its atmospheric and oceanic components. Understanding these sensitivities is necessary to achieve further insight into the mechanisms at work for atmosphere–ocean interactions, as well as to guide improvements in models that attempt to simulate those interactions. For example, there is a general belief that an accurate simulation of the seasonal cycle of the coupled system is crucial for success in simulating ENSO (e.g., Meehl 1990; Jin et al. 1994; Tziperman et al. 1994). And yet, some models that obtain a realistic climatology produce an unrealistically weak interannual variability.

A useful way to look into the sensitivities of the coupled system is to compare simulations performed by a CGCM and by its atmospheric component (AGCM) with prescribed sea surface temperatures (SSTs). This study presents such a comparison in the context of the seasonal cycle of surface heat flux simulated by the University of California, Los Angeles (UCLA) CGCM and AGCM. The differences obtained in simulated surface heat fluxes are then related to those between simulated and prescribed SSTs (i.e., the errors of the CGCM). Although the work reported here is performed in the framework of a particular model, we believe that its conclusions apply to most contemporary coupled GCMs.

We start in section 2 by describing the models used, simulations performed, and datasets selected for verification of results. Section 3 compares the annual cycle of surface heat flux produced by the AGCM, CGCM, and observational estimates. Section 4 focuses on the simulation of SST and latent heat flux over the equatorial cold tongue. Section 5 discusses the mechanisms at work for the simulated annual variations of SST in the equatorial cold tongue. Section 6 summarizes our results and presents our conclusions.

2. Models, simulations, and datasets

The UCLA CGCM used in this study consists of the UCLA global AGCM (Suarez et al. 1983; Kim 1996;

Corresponding author address: Jin-Yi Yu, Department of Atmospheric Sciences, University of California, Los Angeles, 405 Hilgard Ave., Los Angeles, CA 90095-1565.
E-mail: yu@atmos.ucla.edu

and references therein) and the tropical Pacific version of the Geophysical Fluid Dynamics Laboratory Modular Ocean Model (Bryan 1969; Cox 1984; Pacanowski et al. 1991). The AGCM includes the schemes of Deardorff (1972) for the calculation of surface wind stress and surface fluxes of sensible and latent heat; Katayama (1972) for shortwave radiation; Harshvardhan et al. (1987) for longwave radiation; Arakawa and Schubert (1974) for parameterization of cumulus convection; and Kim (1996) for parameterization of gravity wave drag. The model has nine layers in the vertical (with the top at 50 mb) and a horizontal resolution of $4°$ lat $\times$ $5°$ long. The oceanic general circulation model (OGCM) includes the scheme of Mellor and Yamada (1982) for parameterization of subgrid-scale vertical mixing by turbulence processes. The ocean model domain is $30°$S–$50°$N and $130°$E–$70°$W. There are 27 layers in the vertical and depth is constant at 4150 m. The longitudinal resolution is $1°$, and the latitudinal resolution varies gradually from $1/3°$ between $10°$S and $10°$N to almost $3°$ at $30°$S and $50°$N. The CGCM resolution is fairly typical for studies on interannual climate variability (e.g., Mechoso et al. 1995). The surface wind stress and heat flux are calculated hourly by the AGCM, and their daily averages passed to the OGCM. The SST is calculated hourly by the OGCM, and its value at the time of coupling passed to the AGCM. This coupling procedure is also typical of contemporary GCMs.

Two multiyear model simulations were conducted. One is a 4-yr-long integration of the AGCM using SSTs prescribed from a monthly climatology (Alexander and Mobley 1976). The other is an 8-yr-long integration of the CGCM. Our experience with the model suggests that integrations of such length produce useful estimates of the model's mean climate. The initial conditions for the AGCM simulation are taken from the observational analyses corresponding to 1200 UTC 1 October 1982. The initial conditions for the CGCM simulation are taken from a 52-yr-long integration in which the OGCM was initially at rest with temperature and salinity distributions corresponding to the January climatology. We analyze annual and monthly mean distributions of simulated net, latent, sensible, shortwave, and longwave surface heat fluxes, as well as those of simulated SSTs.

The verification dataset for surface winds and heat fluxes is that compiled by Oberhuber (1988) (hereafter "the observation"). This dataset was mainly derived from the Comprehensive Ocean Atmosphere Data Set (Woodruff et al. 1987) for the period 1950–79 and covers most of the global ocean with a resolution of $2°$ lat $\times$ $2°$ long. The verification dataset for surface wind stress corresponds to the monthly fields analyzed at The Florida State University (Legler and O'Brien 1985). All fields were regridded by linear interpolation to the $4°$ lat $\times$ $5°$ long grid of the AGCM for comparisons with the model output.
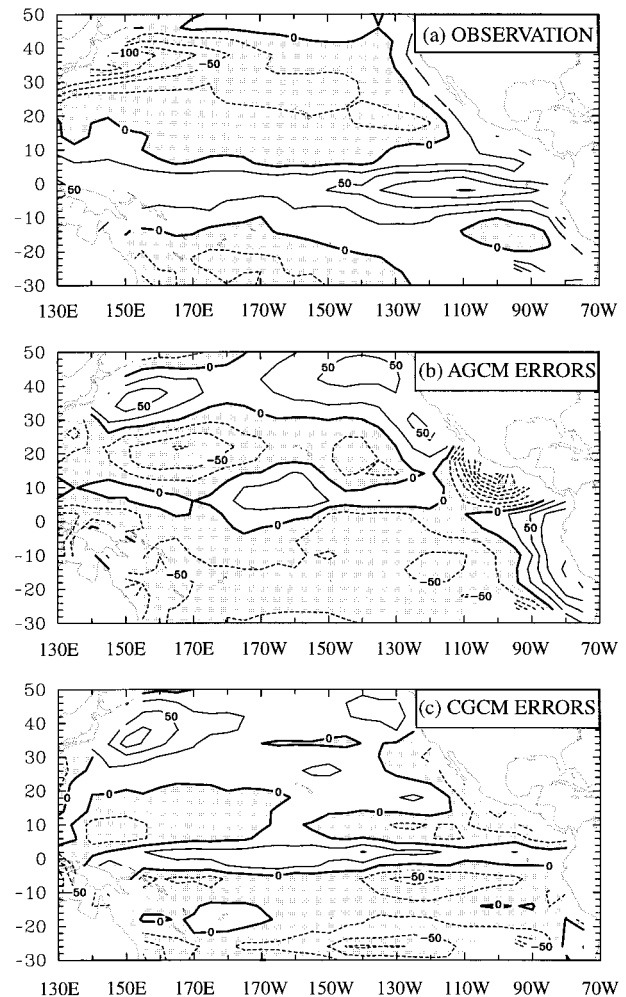

FIG. 1. The annual-mean surface heat flux into the ocean from the observation (a), and errors in annual-mean surface heat flux produced by the AGCM (b) and the CGCM (c). Contour interval is 25 W m^{-2}. Negative values are shaded.

3. Simulations of surface heat flux and SST

Figure 1 shows the annual-mean net surface heat flux in the observation and the errors obtained in the simulations. The net fluxes in the observation are into the ocean around the equator and along the coasts of the Americas, with largest magnitudes (>75 W m^{-2}) over the equatorial cold tongue in the eastern Pacific. Fluxes are out of the ocean almost everywhere else, with largest magnitudes along the coast of Asia. The AGCM produces too strong net heat flux from the ocean in the northern and southern subtropics, and along the coasts of Mexico and Central America. The model also produces too strong heat flux into the ocean along the coasts of California and South America. The CGCM shows a similar error pattern, but with significantly smaller magnitudes. One notable exception is along the equator where AGCM errors are smaller. Another exception is just south of the equator between about $90°$ and $140°$
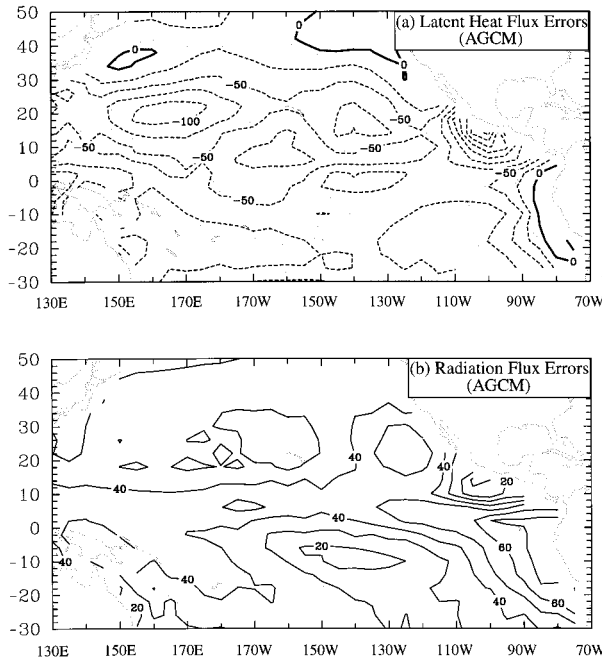
FIG. 2. Errors in annual-mean latent heat (a) and net radiation (b) surface fluxes produced by the AGCM. Contour intervals are 25 and 10 W m^{-2}. Negative values are shaded.

FIG. 4. The differences between the annual-mean surface heat flux produced by the CGCM and the AGCM. Contour interval is 25 W m^{-2}. Negative values are shaded. Labels "a"–"g" identify the centers of regions selected for further analyses.

W, where the coupled model exhibits a problem shared by many contemporary coupled GCM: a spurious southern ITCZ (see Mechoso et al. 1995 for discussion on this issue).
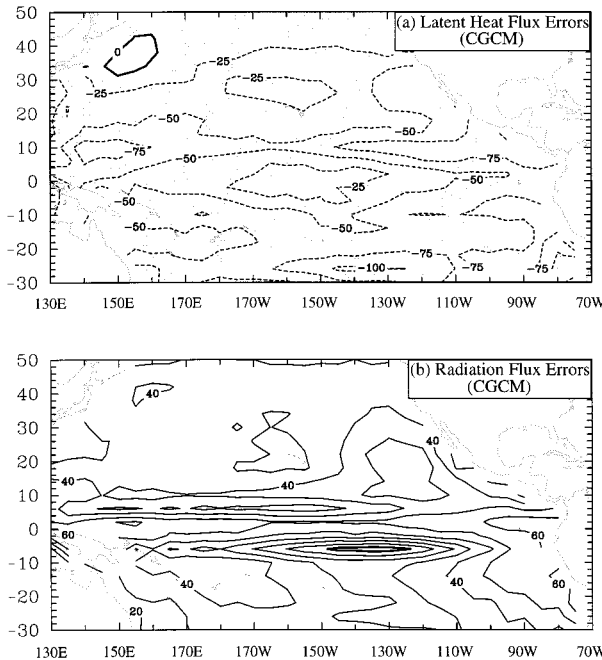
The main contributors to the errors shown in Fig. 1

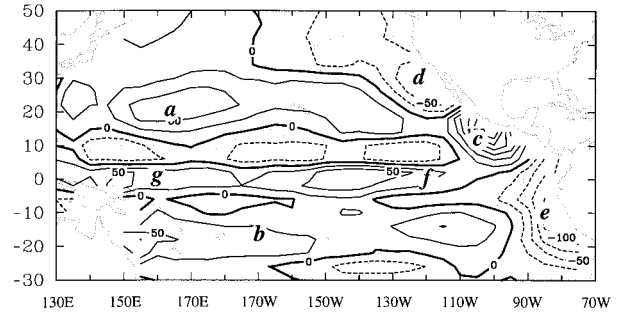FIG. 3. Same as Fig. 2, except for the CGCM.

are deficiencies in the latent and radiative heat fluxes, while those in sensible heat flux are substantial only at higher latitudes and will not be discussed further. Figure 2 displays separately the AGCM errors in annual-mean latent and radiative heat fluxes into the ocean. The model produces excessive evaporation, except along the coasts of California and South America. The model also produces excessive radiative flux into the ocean, particularly along the coast of South America where the shortwave component is too strong (not shown). Note that excessive evaporation along the coast of Mexico and Central America is associated with a local minimum in radiative flux errors due to a spurious enhancement of local cloud cover. Figure 3 is the counterpart of Fig. 2 for the CGCM. The errors in latent heat flux produced by the CGCM are significantly smaller than those produced by the AGCM, while errors in net radiative flux have comparable magnitudes. In the coupled model, the smaller values of net radiative flux errors just south of the equator are associated with the increased cloudiness of the spurious southern ITCZ.

To examine regional features, we plot in Fig. 4 the differences between the annual-mean surface heat flux simulated by the CGCM and AGCM. Off the equator, Fig. 4 shows five regions with local extrema: (i) the northern subtropical Pacific, (ii) the southern subtropical Pacific, (iii) off the coasts of Mexico and Central America, (iv) off the coast of California, and (v) off the coast of Peru.[1] Figure 5 reveals that all five regions under consideration coincide approximately with locations of large SST errors. The CGCM simulates cold SST biases where the AGCM overestimates the heat fluxes *from* the ocean, and warm biases where the AGCM overestimates the fluxes *into* the ocean. In this context, cold SST biases in the CGCM are associated with a lower and more realistic evaporation in regions (a), (b), and (c). On the other hand, the CGCM erroneously increases the evap-

[1] Table 1 presents the extent in longitude and latitude of regions (a), (b), (c), (d), and (e), as well as those of (f) and (g) in Fig. 4.

TABLE 1. Averaging regions in Fig. 4

Region	a	b	c	d	e	f	g
Long	140°E–170°W	180°–160°W	120°W–95°W	130°W–115°W	95°W–75°W	130°W–100°W	150°E–180°
Lat	12°N–28°N	10°S–20°S	8°N–18°N	20°N–36°N	22°S–0°	4°S–4°N	4°S–4°N

oration in association with warm SST biases to balance the too strong downward shortwave radiative flux produced by the AGCM in regions (d) and (e). Note that the shortwave flux in the two models is practically the same, despite the potential for increased convection over warmer surfaces. The tendency toward compensation between differences in surface heat flux and SST produced by the AGCM and CGCM holds both in the annual and monthly means (not shown).

At the equator, Fig. 6 shows that the tendency toward compensation between differences in simulated surface heat flux and SST holds throughout most of the year in the western equatorial Pacific (region ''g''), but not over the equatorial cold tongue (region ''f''). Here, the surface heat fluxes simulated by the AGCM and CGCM differ primarily in their latent heat flux components, and hence in the evaporation. Figure 7 shows the annual variations of monthly mean evaporation and SST from the CGCM and the observation in the equatorial cold tongue. The annual variations simulated by the AGCM are similar to those in the observation (not shown). There are two striking features in the panels of Fig. 7. First, the annual variations of SSTs in the simulation and observation are very similar, which implies a realistic performance of the CGCM. Note, however, that the simulated cold phase of the cold tongue (July–December) is stronger but does not last as long as in the observation. Second, the annual variations of evaporation have large differences. In the observation, evaporation tends to be weaker during the warm phase of the cold tongue (January–June), and stronger during the cold phase. The CGCM simulates a different behavior: evaporation is stronger during the warm phase of the cold tongue, and weaker during the cold phase. In the observation, therefore, surface evaporation contributes to maintain the warm and cold phases of the equatorial
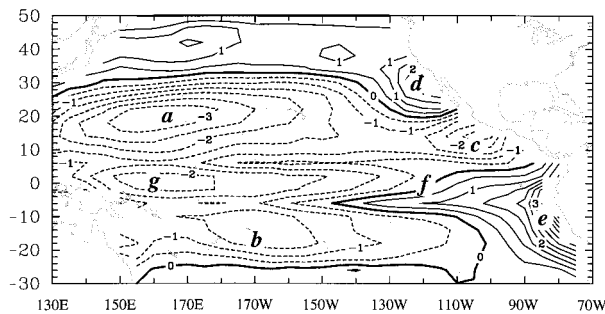

FIG. 5. The errors in annual-mean sea surface temperature simulated by the CGCM. Contour interval is 0.5 K. Negative values are shaded. The regions ''a''–''g'' correspond to those introduced in Fig. 4.

cold tongue. In the CGCM simulation, on the other hand, evaporation tends to damp the annual SST variations in the cold tongue. The feedback between annual variations in evaporation and SST is, therefore, negative in the CGCM and positive in the observation.

4. On the simulation of SST and latent heat flux over the equatorial cold tongue

The latent heat flux in the model and the observation is calculated by using the bulk-aerodynamic formula:

$$L = H\rho_a CV\Delta q, \tag{1}$$

where H is latent heat of condensation; ρ_a and V are air density and wind speed near the surface, respectively; Δq is difference between the saturated specific humidity at a temperature equal to the SST, $q^*(\text{SST})$, and the specific humidity of the overlying air, $q(T_a)$; and C is a transfer coefficient. In the observation, ρ_a, V, and T_a correspond to values measured at the ocean surface; in the AGCM they correspond to the mean values in the planetary boundary layer (PBL). If bars denote annual means, and primes denote deviations from the annual means (i.e., the annual variations), then Eq. (1) can be written in the following way:

$$\frac{L'}{H\rho_a} \approx C'\overline{V}\Delta\overline{q} + \overline{C}\,\overline{V}(\Delta q)' + \overline{C}V'\Delta\overline{q}, \tag{2}$$

where the products of primed quantities are neglected and ρ_a is assumed to be constant. We have verified the validity of the former approximation by comparing the magnitudes of terms retained and neglected in Eq. (2). In all cases, the amplitudes of the annual variations in wind speed and humidity difference are generally less than 30% of the corresponding annual-mean values. To determine the relative contribution to the annual variations of latent heat flux of variations in PBL or surface wind speed, humidity difference across the air–sea interface, and transfer coefficient associated with near-surface turbulence, we recast Eq. (2) in the following way:

$$\frac{L'}{L} \approx \frac{C'}{\overline{C}} + \frac{V'}{\overline{V}} + \frac{(\Delta q)'}{\Delta\overline{q}}. \tag{3}$$

Daily values of C, which are not saved in the AGCM output, were obtained by using Eq. (1) with the appropriate daily means of L, V, and Δq. Since the daily mean values of V can be very small, C was given an upper bound of 3×10^{-3} m² s⁻². The resulting values of C were similar to those obtained in two 1-yr-long AGCM
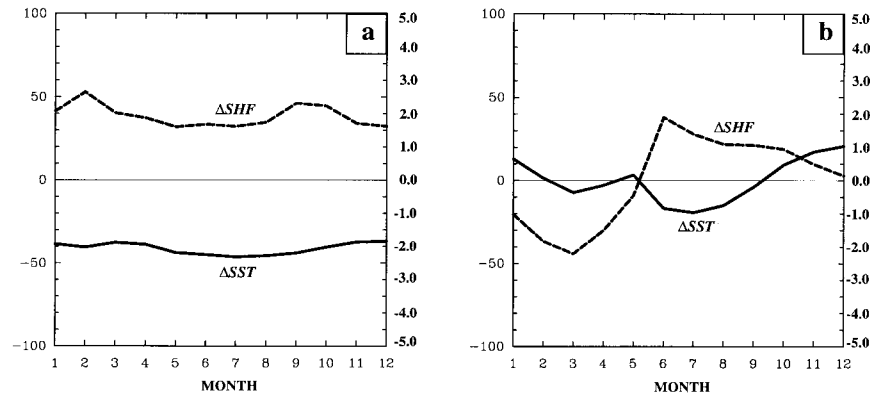
FIG. 6. Annual variations of SST errors (solid) produced by the CGCM and surface heat flux differences (dashed) between the CGCM and the AGCM simulations for (a) the western equatorial Pacific (region ''g'' in Fig. 4) and (b) the equatorial cold tongue (region ''f'' in Fig. 4). The scales of surface heat flux difference (W m^{-2}) are shown on the left axis, and those for SST errors (K) are on the right axis.

and CGCM simulations in which the PBL fields were saved.

The annual variations of the terms in Eq. (3) from the observation and model simulations are displayed in Fig. 8. In all cases, the contribution of transfer coefficient to the annual variations of latent heat flux is small, and will not be discussed further. Figure 8a shows that the humidity difference between ocean surface and overlying air in the observation tends to be larger during the warm phase and smaller during the cold phase of the cold tongue. Also surface wind speed tends to be weaker during the warm phase and stronger during the cold phase of the cold tongue. The magnitudes of annual variations are larger in surface wind speed than in the humidity difference. Therefore, the observed annual variations in latent heat flux are generally in phase with those in surface wind speed. The AGCM broadly reproduces this behavior (Fig. 8b). The CGCM, on the other hand, produces annual variations in latent heat flux that are generally in phase with those in humidity difference (Fig. 8c). This erroneous feature of the CGCM is related to the unrealistically weak annual variations of PBL wind speed, which is almost constant throughout the year.

Although the PBL wind speed in the CGCM has weak annual variations over the equatorial cold tongue, its zonal and meridional components are far from constant (see Fig. 9). The annual variations of zonal wind in the two simulations are quite similar, except that the AGCM obtains systematically stronger easterlies than the CGCM. The simulated meridional winds, on the other hand, are quite different. While the AGCM produces southerlies throughout the year (in agreement with the observation), the CGCM produces northerlies from January through April. Thus, the monthly mean PBL wind speed simulated by the CGCM is almost constant in time because the magnitude of the meridional wind com-

ponent increases spuriously when the magnitude of the zonal wind component decreases realistically.

Finally, we address the reasons for the spurious northerly component of the simulated PBL wind over the equatorial cold tongue during the period January–April. In several CGCMs, this feature is associated either with a spurious migration of the ITCZ to the south of the equator or with the development of an unrealistically strong ITCZ in the Southern Hemisphere (Mechoso et al. 1995). In view of the close association between surface wind and sea level pressure patterns (SLP) around the equator, we present in Fig. 10 the differences between PBL wind and SLP fields simulated by the CGCM and AGCM for March and October. Figure 10 shows that the CGCM consistently produces higher SLP off the coast of Mexico, where simulated SSTs are too cold, and lower SLP off the coast of Peru, where simulated SSTs are too warm. Figure 10 also shows that the gradient of SLP difference across the equator in the eastern equatorial Pacific is much stronger in March than in October. This stronger gradient is consistent with the spurious northerly winds simulated locally by the CGCM during the period January–April.

The differences in the eastern tropical Pacific between the panels of Fig. 10 can be interpreted in light of the evaporative feedback mechanism proposed by Xie (1994) and Robertson et al. (1995). The cold SSTs simulated by the coupled GCM off the coast of Mexico are consistent with the advection of relatively dry, cooler air from the North American continent. This advection is stronger in the northern winter and spring than in the northern summer and fall. The dry and cooler air flowing over the ocean results in large latent heat fluxes from the ocean, which lowers the SSTs. Once the SSTs cool down, deep convection is suppressed, effectively displacing the ITCZ southward. This is consistent with a further drying of the PBL north of the equator as a
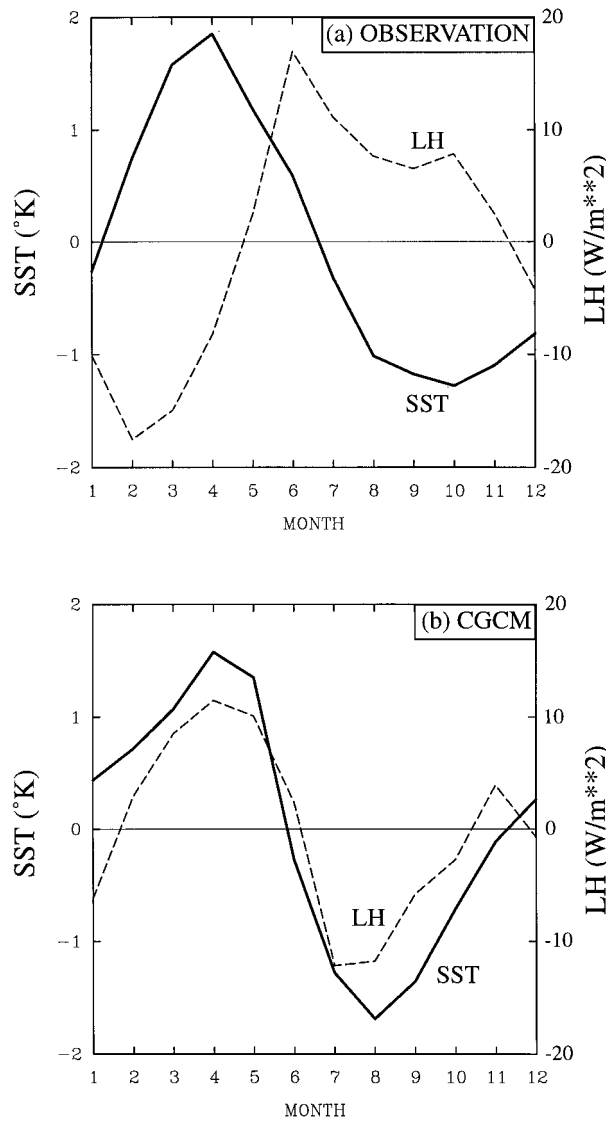
FIG. 7. Annual variations of SST and evaporation averaged over the equatorial cold tongue from (a) the observation and (b) the CGCM simulation.

consequence of turbulent entertainment of air from the free atmosphere, thereby enhancing the process. The ITCZ can eventually cross to the Southern Hemisphere where simulated SSTs are unrealistically high due to the combined effects of underestimated transport of cold water by the Peru current and weak sensible heat flux out of the ocean consistent with weak surface winds (Ma et al. 1995). This, in turn, is associated with underestimated stratus clouds cover off the coast of Peru, which contributes significantly to the overestimated SSTs in that region. The process of cross-equatorial ITCZ migration is schematically shown in Fig. 11.

The existence of this process implies that flaws in the simulations of the eastern equatorial Pacific climate with the CGCM cannot be attributed to deficiencies in the
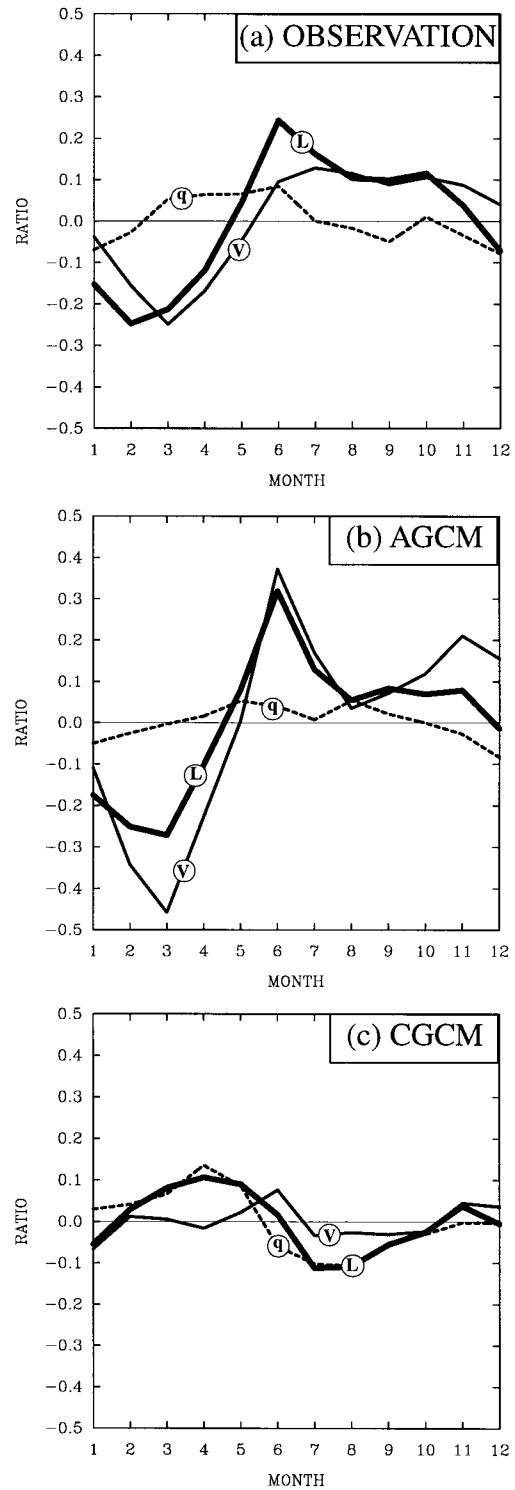

FIG. 8. Contributions to the annual variation of latent heat flux from the annual variations of wind speed and humidity difference obtained from the observation (a) and those produced by the AGCM (b) and CGCM (c). The labels "L" indicate the seasonal cycles of the term $L'/\overline{L}$ in Eq. (3), "q" for the term $(\Delta q)'/\Delta \overline{q}$, and "V" for the term $V'/\overline{V}$.
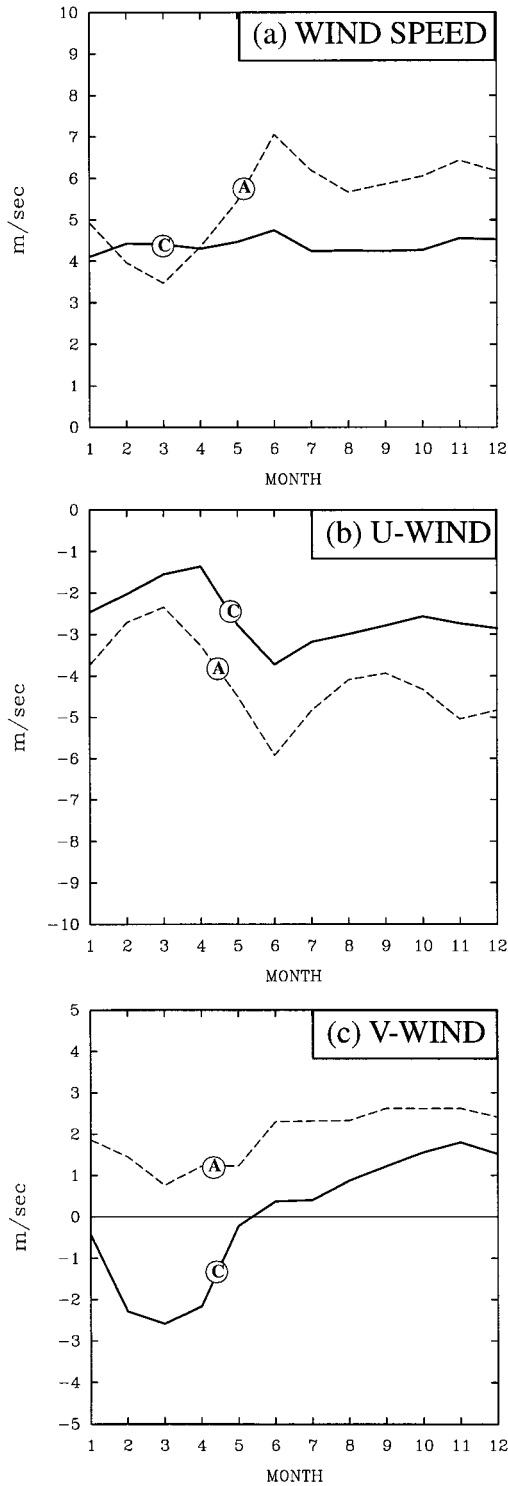
FIG. 9. Annual march of monthly mean (a) wind speed and (b) zonal and (c) meridional winds averaged in the PBL over the equatorial cold tongue. Curves labeled "A" and "C" correspond to the simulations by the AGCM and CGCM, respectively.

representation of a single physical process, and are rather due to a combination of errors amplified by the feedbacks of the coupled system. The AGCM resolution is coarse and the soil conditions along the coast are poorly resolved. Off the coasts of California and Mexico, this implies that airflows over the ocean just downstream of a continental surface whose soil conditions correspond to inland deserts. This dry air is consistent with high evaporation from the ocean surface. In addition, the oceanic stratus clouds were seriously underestimated in the AGCM. Ma et al. (1995) found that Peruvian stratocumulus clouds are important in modulating the climate of the tropical Pacific, not only along the coast of Peru but also south of the equator where simulated SSTs tend to have a warm bias. Lastly, the parameterizations of deep convection and PBL processes in the AGCM may be especially, albeit realistically, sensitive to overestimated SST. In this way, convection over the eastern Pacific develops south of the equator, which is too warm due to deficiencies in the simulation of Peruvian stratocumulus clouds.

5. On the mechanisms at work for the simulated annual variations of SST in the equatorial cold tongue

We indicated in section 4 that the CGCM simulates realistic annual variations of SST and unrealistic annual variations of latent heat fluxes in the equatorial cold tongue. Nigam and Chao (1996) pointed out that latent heat fluxes have modest magnitude over the cold tongue, although their positive tendency leads SST cooling in the off-coastal zone. In this section, we examine the annual variations of SST, zonal and meridional wind stress, and shortwave flux at the equator from the date line to the South American coast, from the CGCM simulation and the observation.

Figure 12 displays the warm and cold phases of the cold tongue, and their westward propagation. The variations of SST are dominated by the annual harmonic that peaks at about 100°W. Near the coast, Fig. 12 shows that the annual variations of shortwave flux at the surface in the observation are largest around the March equinox, and smallest around the September equinox. The peak values are similar to those for clear skies in the tropical Pacific (Wang 1994). The different surface fluxes at the equinoxes are primarily due to different cloudiness over warmer and colder waters. The CGCM produces a very different behavior. The simulated shortwave fluxes are small in March and peak in September. The small values in March are mostly due to an overestimation of the amount of deep clouds associated with warmer SSTs. The erroneous peak in September is consistent with the poor simulation of low-level clouds above colder SSTs. Away from the coast, there are similarities between the annual variations of shortwave flux at the surface in both the observation and simulation as conditions are closer to those prevailing under clear
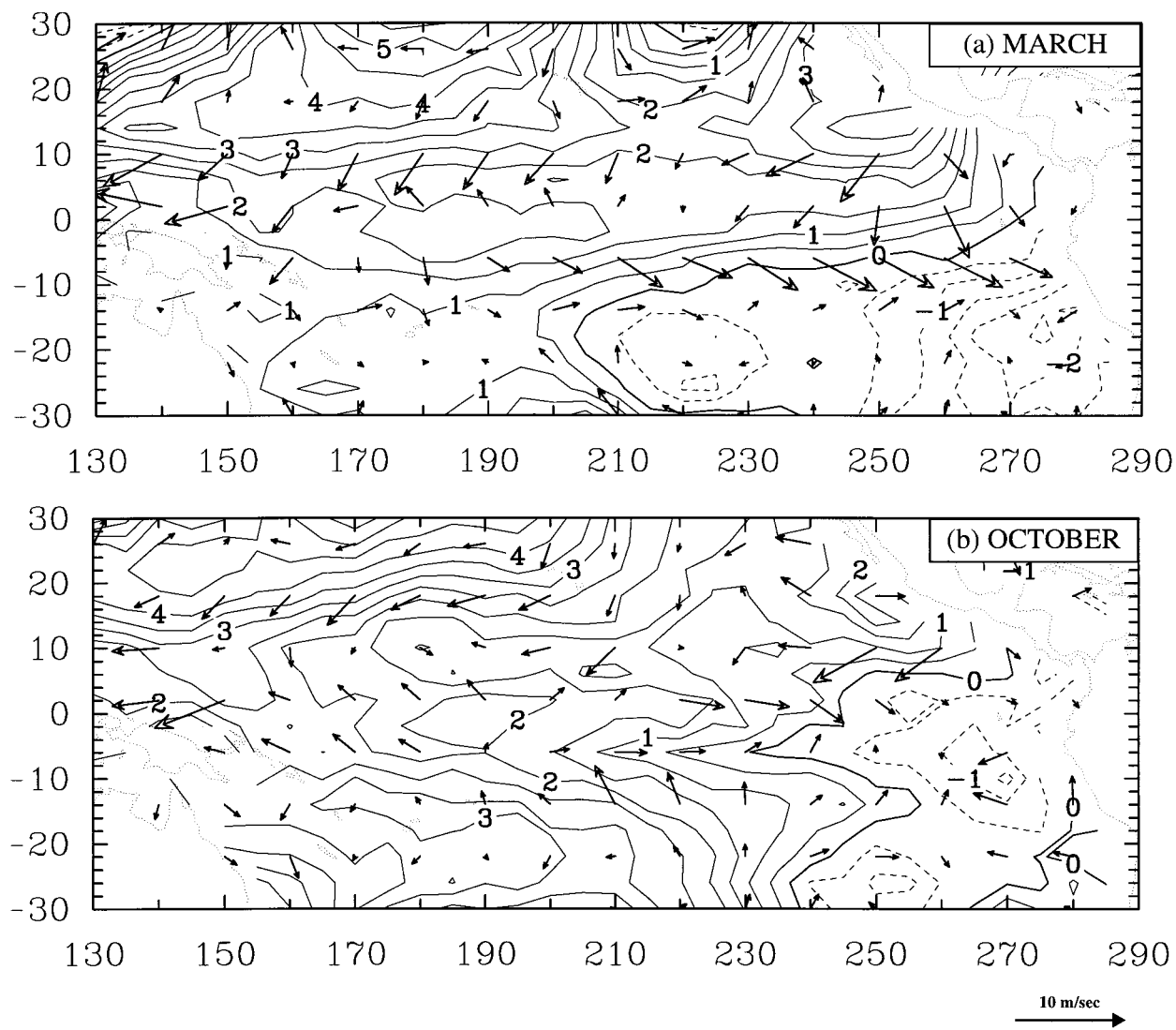
FIG. 10. Differences between sea level pressure (contours) and PBL-wind (vectors) simulated with the CGCM and those simulated with the AGCM in (a) March and (b) October. The contour interval for sea level pressure differences is 0.5 mb. Wind vectors are plotted at every other model grid point.

skies. These results support the notion that annual variations in shortwave flux at the surface over the equatorial cold tongue are not the primary drivers of the corresponding variations in SST. Near the coast, the erroneous low values simulated at the March equinox are consistent with a weaker warm phase and the erroneous peak at the September equinox contributes to the earlier termination of the cold phase. The erroneous latent heat flux discussed in the previous section of this paper is another contributor to this earlier termination.

Next we focus on the wind stress at the surface. The meridional component in both the observation and simulation shows positive values in the second half of the year and negative values in the first half of the year. In the observation, however, the minimum values around March correspond to the weakest southerlies of the year,

while in the simulation they correspond to the strongest northerlies of the year and the zero values approximately correspond to zonal flow. Near the coast, therefore, the observation shows weak southerlies around the March equinox and strong southerlies around the September equinox. This pattern of annual variations is consistent with the monsoonal circulation developing over Colombia and Central America. Mitchell and Wallace (1992) hypothesize that such an increase, centered at the northern fringe of the equatorial wave guide, can start a series of coupled atmosphere–ocean feedback processes that promote upwelling in the cold tongue. The simulation is in general agreement with this scenario during the cold phase of the cold tongue. The warm phase, however, shows strong northerlies and easterlies that are associated with the flow diverging from the SLP center
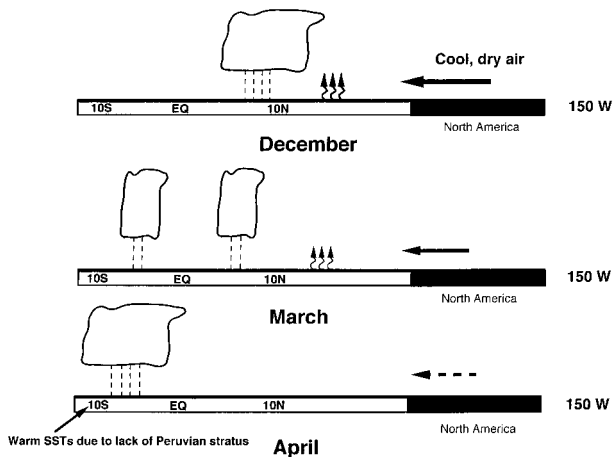
FIG. 11. A schematic showing how the evaporation feedback mechanism contributes to the cross-equatorial migration of the ITCZ in the CGCM simulation.

west of Mexico, where simulated SSTs are too cold (see Fig. 10). This pattern of wind stress is consistent with decreased upwelling and higher SSTs in the cold tongue where shortwave fluxes are weak.

Off the coast, the annual variations of zonal wind stress are consistent with those in the seasonally varying Hadley circulations. Schneider and Zhu (1998) point out that at the equator the zonal wind in a zonally symmetric model is expected to be negatively correlated with the intensity of the Hadley circulation. A stronger Hadley circulation at the equator would be associated with stronger easterlies because higher speeds of the meridional wind imply stronger advection of air whose angular momentum is representative of latitudes further away from the equator. In this context, both observation and simulation show increased easterlies and colder SSTs in the second half of the year.

The annual variations of SSTs in the equatorial cold tongue, therefore, appear consistent with those in equatorial wind stress and associated upwelling. Near the coast, the variations of meridional wind stress are broadly consistent with those expected in association with the monsoonal circulations. The warm phase produced by the CGCM, however, is also partially affected by compensating effects of errors in wind stress and surface heat flux. Off the coast, the equatorial easterlies and westerlies consistent with the cold and warm phases of the cold tongue seem associated with the variable intensity of the seasonally varying Hadley circulation.

6. Summary and conclusions

We have compared the surface heat flux in the tropical Pacific simulated by the UCLA CGCM and AGCM, and the SST in the CGCM simulation and the observation. The study emphasizes regional errors in those fields. Off the equator, the AGCM overestimates the heat flux out of the ocean in the northern and southern subtropics and along the coast of Mexico and Central America; these errors are primarily due to excessive evaporation. The model also overestimates the heat flux into the ocean along the coasts of California and South America; these errors are primarily due to excessive downward shortwave radiation. The CGCM produces much small surface heat flux errors in those regions. However, the CGCM simulates cold and warm SST biases where the AGCM overestimates the heat fluxes from and into the ocean, respectively. The surface heat flux errors produced by AGCM deficiencies, therefore, tend to be compensated in the CGCM by SST errors. This compensation relationship suggests that interactions between surface heat flux and SST on monthly timescales off the equator are local.

Over the western equatorial Pacific, the AGCM produces realistic values of surface heat flux. The CGCM, on the other hand, produces a cold SST bias. This error is a manifestation of a spuriously elongated cold tongue, which is a common deficiency of contemporary CGCMs. Since this phenomenon is primarily due to coupled atmosphere–ocean dynamical processes, there is not a straightforward connection between surface heat flux and SST errors.

Over the eastern equatorial Pacific, ocean dynamics plays a key role in SST variations. The compensation between CGCM errors in SST and AGCM errors in surface heat flux does not hold here. Moreover, the annual variations of latent heat flux are realistically simulated by the AGCM but not by the CGCM. In both the observation and AGCM simulation, the annual variations in latent heat flux are approximately in phase with those in surface or PBL wind speeds. In the CGCM simulation, however, the variations are in phase with those in the humidity difference between ocean surface and overlying air. This erroneous feature of the CGCM was shown to be associated with the spurious northerly wind simulated over the cold tongue in the late northern winter and spring.

Despite the problems found in the CGCM performance, the model produces a fairly realistic simulation of the annual variations in SST in the equatorial cold tongue. This finding agrees with the notion that annual variations of latent heat flux play a secondary role in the phenomenon in question. Our results also support the concept that the monsoonal circulation plays a key role in the annual variations of the cold tongue, particularly during its cold phase. Even in CGCMs whose atmospheric components have a relatively low horizontal resolution similar to that used in this study, one would expect to resolve the major features in the seasonal evolution of tropical convection. In this context, the broad aspects of the annual variations of the equatorial cold tongue, particularly the existence and duration of its cold phase, can be relatively easy to simulate with a CGCM. In fact, 7 of the 11 models examined in Mechoso et al. (1995) show a realistic performance in this regard. A comparable success for the warm phase

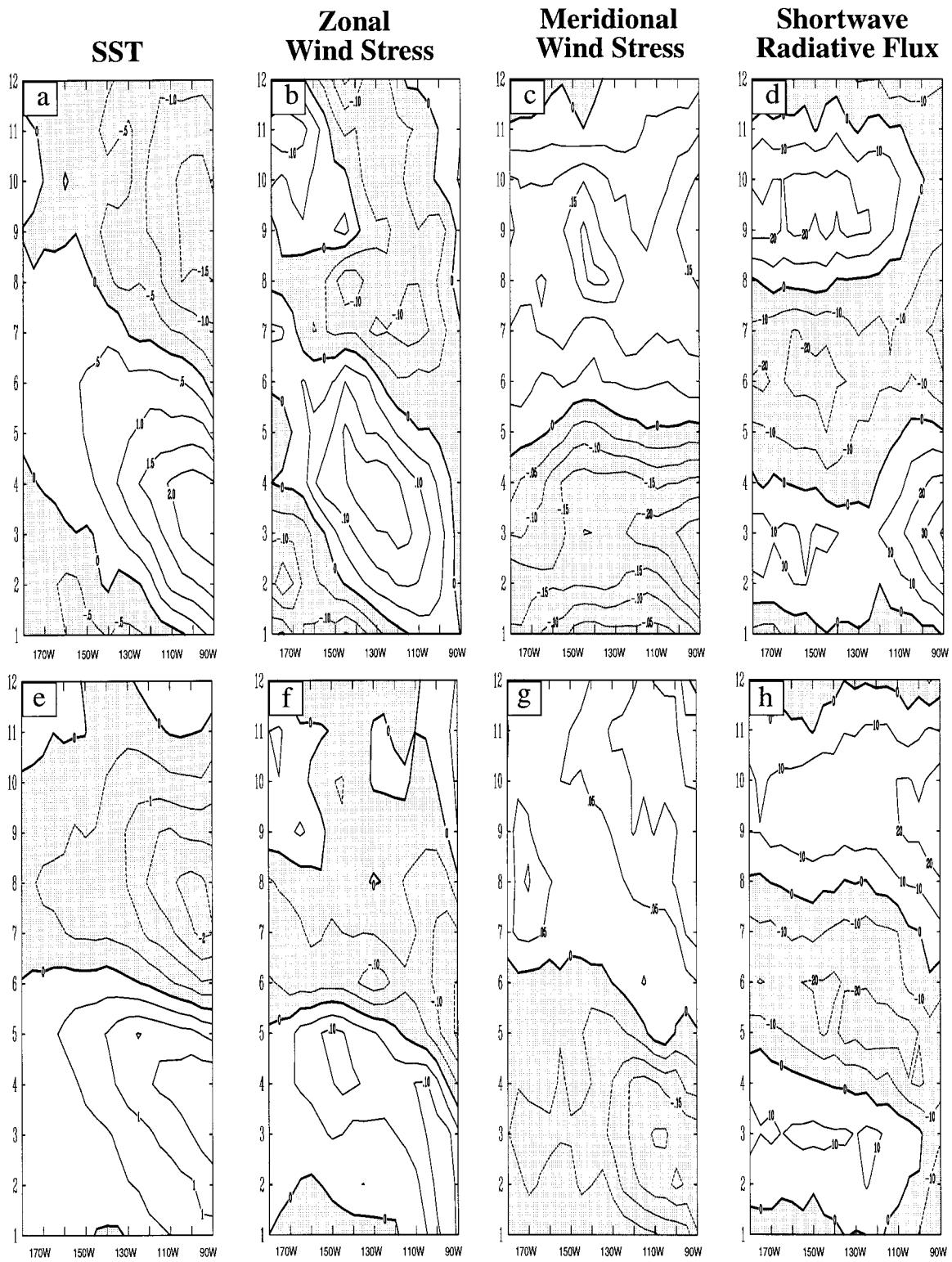**SST** **Zonal Wind Stress** **Meridional Wind Stress** **Shortwave Radiative Flux**

FIG. 12. Annual variations along the central to eastern equatorial Pacific in the observed (a) SST, (b) zonal wind stress, (c) meridional wind stress, and (d) surface shortwave radiative flux. The variations simulated by the CGCM are shown in (e) for SST, (f) for zonal wind stress, (g) for meridional wind stress, and (h) for shortwave radiative flux. Values shown are averaged between 4°S and 4°N. Contour intervals are 0.5°C for (a) and (e), 0.05 dyn cm² for (b), (c), (f), and (g), and are 10 w m² for (d) and (h).

is more elusive. Once again, our results are consistent with the notion that unrealistic features in the simulation of the eastern tropical Pacific climate by a CGCM may not be attributed to deficiencies in the representation of a single physical process, but are rather due to a combination of errors amplified by feedbacks of the coupled system.

Since the time that this manuscript was completed, a major revision of the PBL parameterization in the UCLA AGCM has resulted in a substantial improvement in the simulated surface heat fluxes. The revised version of the uncoupled AGCM also produces a realistic simulation of marine stratocumulus and subsequent reduction of shortwave fluxes in the appropriate regions. A coupled model using this revised version of the AGCM obtained a much more realistic mean climate in the subtropics and an improved interannual variability at the equator (Yu and Mechoso 1998). The general conclusions of this study remain nevertheless valid.

REFERENCES

Alexander, R. C., and R. L. Mobley, 1976: Monthly average sea-surface temperatures and ice pack limits on a 1° global grid. *Mon. Wea. Rev.,* **104,** 143–148.

Arakawa, A., and W. H. Schubert, 1974: Interaction of a cumulus cloud ensemble with the large-scale environment, Part I. *J. Atmos. Sci.,* **31,** 674–701.

Bryan, K., 1969: A numerical method for the study of the circulation of the world ocean. *J. Comput. Phys.,* **4,** 347–376.

Cox, M. D., 1984: A primitive equation three-dimensional model of the ocean. GFDL Ocean Group Tech. Rep. 1, NOAA/GFDL, Princeton, NJ, 75 pp. [Available from GFDL/NOAA, Princeton University, Princeton, NJ 08540.]

Deardorff, J. W., 1972: Parameterization of the planetary boundary layer for use in general circulation models. *Mon. Wea. Rev.,* **100,** 93–106.

Harshvardhan, D. A. Randall, and T. G. Corsetti, 1987: A fast radiation parameterization for general circulation models. *J. Geophys. Res.,* **92,** 1009–1016.

Jin, F.-F., J. D. Neelin, and M. Ghil, 1994: El Niño on the devil's staircase: Annual subharmonic steps to chaos. *Science,* **264,** 70–72.

Katayama, A., 1972: A simplified scheme for computing radiative transfer in the troposphere. Numerical Simulation of Weather and Climate Tech. Rep. 6, 77 pp. [Available from Dept. of Atmospheric Sciences, University of California, Los Angeles, Los Angeles, CA 90024.]

Kim, Y.-J., 1996: Representation of subgrid-scale orographic effects in a general circulation model. Part I: Impact on the dynamics of simulated January climate. *J. Climate,* **9,** 2698–2717.

Legler, D. M., and J. J. O'Brien, 1985: Atlas of tropical Pacific wind stress climatology 1971–1980. Dept. of Meteor., The Florida State University, Tallahassee, FL, 182 pp. [Available from Department of Meteorology, The Florida State University, Tallahassee, FL 32306-3041.]

Ma, C.-C., C. R. Mechoso, A. W. Robertson, and A. Arakawa, 1996: Peruvian stratus clouds and the tropical Pacific circulation: A coupled ocean–atmosphere GCM study. *J. Climate,* **9,** 1635–1645.

Mechoso, C. R., and Coauthors, 1995: The seasonal cycle over the tropical Pacific in general circulation models. *Mon. Wea. Rev.,* **123,** 2825–2838.

Meehl, G. A., 1990: Seasonal cycle forcing of El Niño–Southern Oscillation in a global coupled ocean–atmosphere GCM. *J. Climate,* **3,** 72–98.

Mellor, G. L., and T. Yamada, 1982: Development of a turbulence closure model for geophysical fluid problems. *Rev. Geophys. Space Phys.,* **20,** 851–875.

Mitchell, T. P., and J. M. Wallace, 1992: On the annual cycle in equatorial convection and sea surface temperature. *J. Climate,* **5,** 1140–1156.

Nigam, S., and Y. Chao, 1996: Evolution dynamics of tropical ocean-atmosphere annual cycle variability. *J. Climate,* **9,** 3187–3205.

Oberhuber, J. M., 1988: An atlas based on the COADS dataset: The budgets of heat buoyancy and turbulent kinetic energy at the surface of the global ocean. Max-Plank-Institut für Meteorologie Rep. 15, 238 pp. [Available from MPI, Bundesstrasse 55, 2000 Hamburg 13, Germany.]

Pacanowski, R. C., K. W. Dixon, and A. Rosati, 1991: The GFDL Modular Ocean Model user guide. Tech. Rep. 2, NOAA/GFDL, Princeton, NJ, 75 pp. [Available from GFDL/NOAA, Princeton University, Princeton, NJ 08540.]

Robertson, A. W., C.-C. Ma, C. R. Mechoso, and M. Ghil, 1995: Simulation of the tropical Pacific climate with a coupled ocean-atmosphere general circulation model. Part I: The seasonal cycle. *J. Climate,* **8,** 1178–1198.

Schneider, E., and Z. Zhu, 1998: Sensitivity of the simulated annual cycle of sea surface temperature in the equatorial Pacific to sunlight penetration. *J. Climate,* **11,** 1932–1950.

Suarez, M. J., A. Arakawa, and D. A. Randall, 1983: The parameterization of the planetary boundary layer in the UCLA general circulation model: Formulation and results. *Mon. Wea. Rev.,* **111,** 2224–2243.

Tziperman, E., L. Stone, H. Jarsoh, and M. A. Cane, 1994: El Niño chaos: Overlapping of resonances between the seasonal cycle and Pacific ocean–atmosphere oscillator. *Science,* **264,** 72–74.

Wang, B., 1994: On the annual cycle in the tropical eastern central Pacific. *J. Climate,* **7,** 1926–1942.

Woodruff, S. D., R. J. Slutz, R. L. Jenne, and P. M. Stenrer, 1987: A comprehensive ocean–atmosphere dataset. *Bull. Amer. Meteor. Soc.,* **68,** 1239–1250.

Xie, S.-P., 1994: The maintenance of an equatorially asymmetric state in a hybrid coupled GCM. *J. Atmos. Sci.,* **51,** 2602–2612.

Yu, J.-Y., and C. R. Mechoso, 1998: Simulations of tropical climate and variability with the UCLA coupled atmosphere–ocean GCM. *Proc. 1998 Conf. on Mission Earth: Modeling and Simulation of the Earth System,* San Diego, CA, Soc. Computer Simulation Int., 3–8.